

This is the initial submission version of the paper

Common dynamo scaling in slowly rotating young and evolved stars (Lehtinen et al. 2020).

The final accepted version can be found at

<https://www.nature.com/articles/s41550-020-1039-x>

Universal dynamo scaling in young and evolved stars

Jyri J. Lehtinen^{1,2}, Federico Spada¹, Maarit J. Käpylä^{2,1}, Nigul Olsper¹ & Petri J. Käpylä^{3,2}

¹*Max Planck Institute for Solar System Research, 37077 Göttingen, Germany*

²*Department of Computer Science, Aalto University, PO Box 15400, FI-00076 Aalto, Finland*

³*Institut für Astrophysik, Georg-August-Universität Göttingen, 37077 Göttingen, Germany*

Activity caused by surface magnetism is a pervasive feature of cool late-type stars where a dynamo mechanism is supported in the outer convective envelopes of the stellar interiors. The detailed mechanism responsible for this dynamo is still debated but its basic ingredients include convective turbulence and non-uniformities in the stellar rotation profile¹, although the role of the former divides opinions. Both the observed surface magnetic fields² and activity indicators from the chromosphere³ to the transition region⁴ and corona⁵ are known to be closely connected with the stellar rotation rate. These relationships have been intensely studied in recent years, some works indicating that the activity should be related to the Rossby number^{5,6}, quantifying the stellar rotation in relation to the convective turnover time, while others claim that the tightest correlation can be achieved using the rotation period alone^{7,8}. Here we tackle this question by including evolved giant stars to the analysis of the rotation–activity relation. These stars rotate very slowly compared to the main sequence stars, but still show strikingly similar activity levels⁹. We show that by using the Rossby number, the two stellar populations fall together in the rotation–activity diagram, and follow the same activity scaling. This suggests that turbulence has a key role in driving stellar dynamos, and that there appears to be a universal turbulence-related dynamo mechanism explaining magnetic activity levels of both main sequence and evolved stars.

A common practice in studies of stellar activity^{3–6} and magnetism^{2,10} has been to assume that the scaling of the activity level is best explained by the Rossby number $Ro = P_{\text{rot}}/\tau_c$, which is the ratio between the stellar rotation period P_{rot} and the convective turnover time τ_c . This interpretation has, however, been contested recently^{7,8}. The main point of criticism against the use of the Rossby number has been that determining its value requires the knowledge of the convective turnover time in the interior of a star. Since this is not a directly observable quantity, it has to be estimated instead using stellar structure models¹¹ or empirical fits³, which increases the risk of introducing systematic errors in the analysis. On the main sequence stars the coronal X-ray luminosity has been noted to be empirically correlated with the rotation period⁷ as $L_X \propto P_{\text{rot}}^{-2}$. Equivalently, the ratio of the X-ray to bolometric luminosity has been related to the rotation period and stellar radius as $L_X/L_{\text{bol}} \propto P_{\text{rot}}^{-2}R^{-4}$, resulting in a marginally better fit than when relating L_X/L_{bol} to empirical Ro of the same stars⁸.

Resolving this controversy on the capability of the Rossby number for correctly describing the activity scaling is important, as it gives direct clues on the dynamo type that is operational in the stellar convection zones. Stellar dynamos depending solely on the rotation period could

indicate preference for Babcock-Leighton-type dynamos, where a crucial part of the dynamo action relies on rising flux tubes becoming twisted by the Coriolis force due to rotation^{12–14}. The rival theory of turbulent dynamos relies on the generation of magnetic fields by rotationally affected convective cells¹⁵. In this case the activity level should also critically depend on the properties of the turbulence, such as the convective turnover time. Hence, the relevant parameter for such dynamos is the Rossby number which describes the rotational influence on convective turbulence¹⁶.

Stars develop increasingly thick convective envelopes as they evolve off the main sequence. As a result the value of τ_c will start to increase once the star reaches the end of its main sequence phase and starts to turn into a giant¹¹. As P_{rot} will continue to increase over time¹⁷ due to magnetic braking and expanding stellar radius, the values of Ro and P_{rot} evolve differently after the end of the main sequence phase. This offers a possibility to test which of the proposed rotation–activity scaling relations works the best once both main sequence and evolved stars are studied in conjunction.

A suitable data set for this study is provided by the chromospheric time series collected during the Mount Wilson Observatory (MWO) Calcium HK Project¹⁸. These data allow straightforward derivation of P_{rot} and the average ratio of the Ca II H&K line core emission to bolometric flux, $R'_{\text{HK}} = F'_{\text{HK}}/F_{\text{bol}}$. This activity index, commonly expressed in the logarithmic form $\log R'_{\text{HK}}$, quantifies the efficiency with which the full energy output of a star is converted to chromospheric heating. The turnover times, τ_c , needed for calculating Ro, were derived from stellar structure models¹⁹, by fitting the model evolutionary tracks to the observed parameters of each star. The Hertzsprung-Russell diagram of the stellar sample is shown in Figure 1 together with the model tracks and isocontours of the resulting τ_c values.

In Figure 2 we show the emission ratio $\log R'_{\text{HK}}$ of the MWO stars against both P_{rot} and Ro. The stars are colour-coded by their observed surface gravity, $\log g$, to indicate their evolutionary phase, main sequence stars having high $\log g$ and the evolved stars low $\log g$. Against P_{rot} the stars are clearly split into two distinct groups, with the evolved stars showing periods of 10 to 100 times longer than main sequence stars of comparable activity levels. Likewise, within the main sequence there is substantial scatter between the least and most massive stars, as seen from the gradient between the least massive ones at $\log g > 4.5$ and the most massive ones at $\log g < 4.0$. When displayed against Ro, on the other hand, the spread disappears and the stars collapse into a single rotation–activity sequence, irrespective of their mass or evolutionary stage.

There is still residual scatter remaining in the calculated Ro values, which needs to be discussed before evaluating the performance of the Rossby number as an activity scaling parameter. This scatter can be attributed largely to model uncertainties in deriving the τ_c values from the structure model fits. In Figure 3 we show $\log R'_{\text{HK}}$ against $\log \text{Ro}$ for all the stars for which an evolutionary track could be fitted. There are a considerable amount of outliers with sizable uncertainties to the large Ro side of the main bulk of the stars. These points mostly correspond to

the stars with the shortest convective turnover times at $\tau_c < 5$ d, as shown by the open symbols in Figure 3. The stars in question are located in the Hertzsprung-Russell diagram very near to the limit where the outer convection zone first appears as intermediate-mass stars ($\approx 2M_\odot$) evolve from the main sequence to the subgiant phase (cf. the $\tau_c = 0$ d contour in Figure 1). This limit remains poorly constrained, and thus the derived thickness of the convection zone near it is highly sensitive to model uncertainties and errors in the stellar parameters. For this reason we excluded the stars with $\tau_c < 5$ d from our analysis as unreliable points. The scatter among the remaining stars is related largely to the subgiant phase, as can be expected due to the short evolutionary timescale of the depth of the convection zone and τ_c during these phases¹¹. The main sequence and giant stars are in much better agreement with each other.

The capability of the different parameters to explain the rotation-activity scaling can be further investigated through Gaussian clustering by finding the optimal configuration of bivariate Gaussian distributions to describe the data. Against P_{rot} this analysis leads to two distinctly separate clusters for the main sequence and evolved stars, while against Ro it favours a single narrow cluster with a broad overlapping secondary cluster, related to the more uncertain τ_c values (Extended Data Figure 1 a,b). Most of both the main sequence and evolved stars fall neatly inside the narrow core cluster, which demonstrates that the Rossby number is indeed a sufficient parameter for explaining the activity scaling of both of these evolutionary stages.

In contrast, alternative activity scaling relations, L_{HK} vs. P_{rot} and R'_{HK} vs. $P_{\text{rot}}^{-2}R^{-4}$, that remove the τ_c dependence from the scaling^{7,8}, fail at closing the gap between the main sequence and evolved stars (Figure 4). Both of these choices show a reasonably good rotation-activity relation for the main sequence stars, but the evolved stars form again their own separate clusters that do not coincide with the main sequence stars (Extended Data Figure 1 c,d).

A further quantitative comparison is possible between the $\log R'_{\text{HK}}$ vs. $\log \text{Ro}$ and the $\log R'_{\text{HK}}$ vs. $\log P_{\text{rot}}^{-2}R^{-4}$ clustering results since in both cases it is possible to express the scatter of the clusters along $\log R'_{\text{HK}}$. Against Ro we find the root mean square scatter to be $\text{rms} = 0.114$ dex in $\log R'_{\text{HK}}$ for the main cluster. This compares with a scatter of $\text{rms} = 0.209$ dex for the main sequence stars and $\text{rms} = 0.120$ dex for the evolved stars against $P_{\text{rot}}^{-2}R^{-4}$. While the difference is minimal for the evolved stars, the main sequence stars show notably worse scatter when scaled against $P_{\text{rot}}^{-2}R^{-4}$.

All these results constitute a strong argument that the Rossby number provides a necessary, as well as sufficient, parametrisation for the stellar activity level over a wide range of evolutionary stages. The resulting scaling relation from the clustering analysis is $R'_{\text{HK}} \propto \text{Ro}^{-0.97}$. Using other proposed parameterisations still allows the construction of empirical rotation-activity relations for the main sequence stars, but these are of poorer quality and break down once more evolved stars are introduced into the picture. The fact that a unified scaling can only be achieved when both stellar rotation and convection are taken into account suggests that the underlying dynamos operating

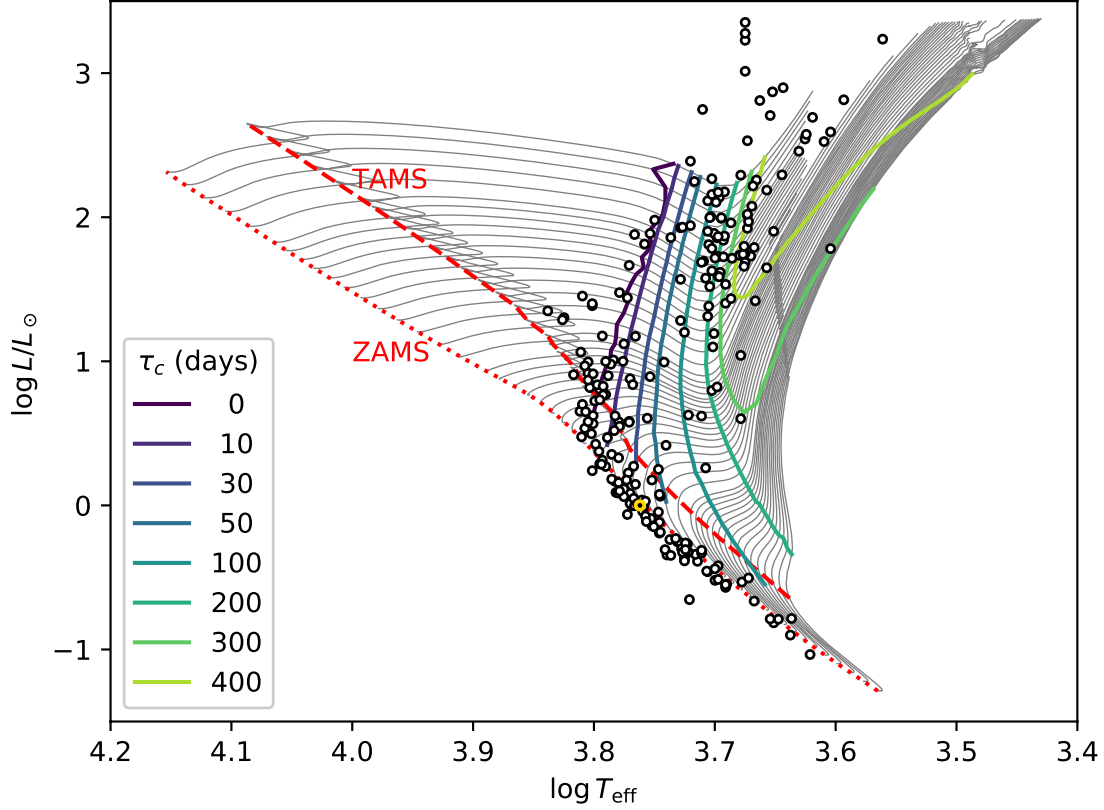


Figure 1: Hertzsprung-Russell diagram of the stellar sample. The stars are shown together with a subset of the model evolutionary tracks used to determine their convective turnover times, τ_c . Only the solar metallicity tracks are shown here for clarity. The red dotted and dashed lines mark the zero age main sequence (ZAMS) and the termination age main sequence (TAMS), respectively, while τ_c isocontours are shown as solid colored lines. The Sun is indicated by the yellow circle.

in these stars follow the turbulent dynamo paradigm. Moreover, also fully convective M-dwarfs have been shown to follow a common rotation-activity relation against Ro together with the more massive partially convective Solar-type main sequence stars^{20–22}. It is thus reasonable to assume that there exists a universal dynamo scaling for all late type stars and that they all share the same underlying dynamo mechanism irrespective of their mass or evolutionary stage and the resulting vastly different internal structures.

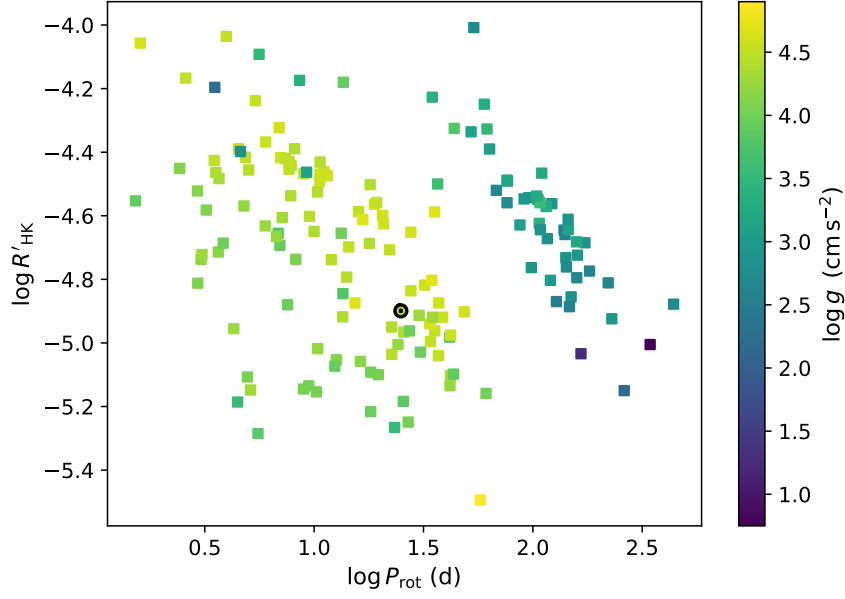
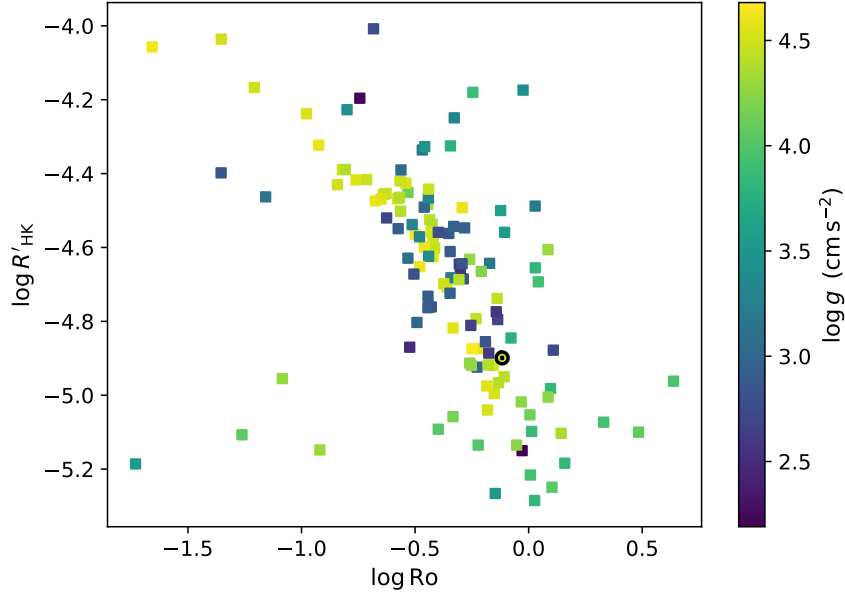
a**b**

Figure 2: Rotation–activity relation for main sequence and evolved stars. **a**, Chromospheric activity, $\log R'_{\text{HK}}$, vs. rotation period, P_{rot} . **b**, Chromospheric activity, $\log R'_{\text{HK}}$, vs. Rossby number, $\text{Ro} = P_{\text{rot}}/\tau_{\text{c}}$. The colour scale denotes the surface gravity, $\log g$, of the stars, distinguishing main sequence stars (yellow to light green) from the evolved stars (dark green to blue).

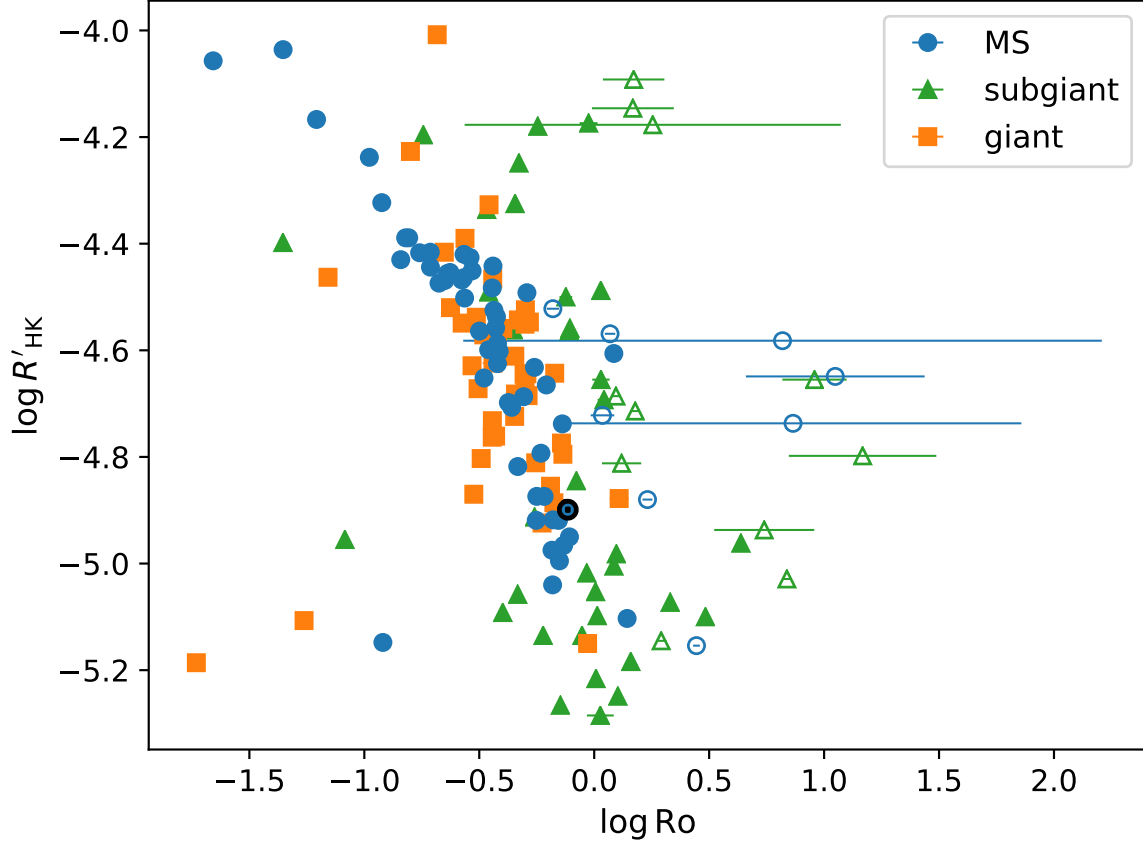


Figure 3: Rotation–activity relation including uncertainties for Rossby number. Stars excluded from the analysis due to the uncertainty in recovering short turnover times ($\tau_c < 5$ d) are shown with open symbols. The error bars indicate the estimated Ro uncertainties and different plot symbols are used for the main sequence (MS), subgiant, and giant stars.

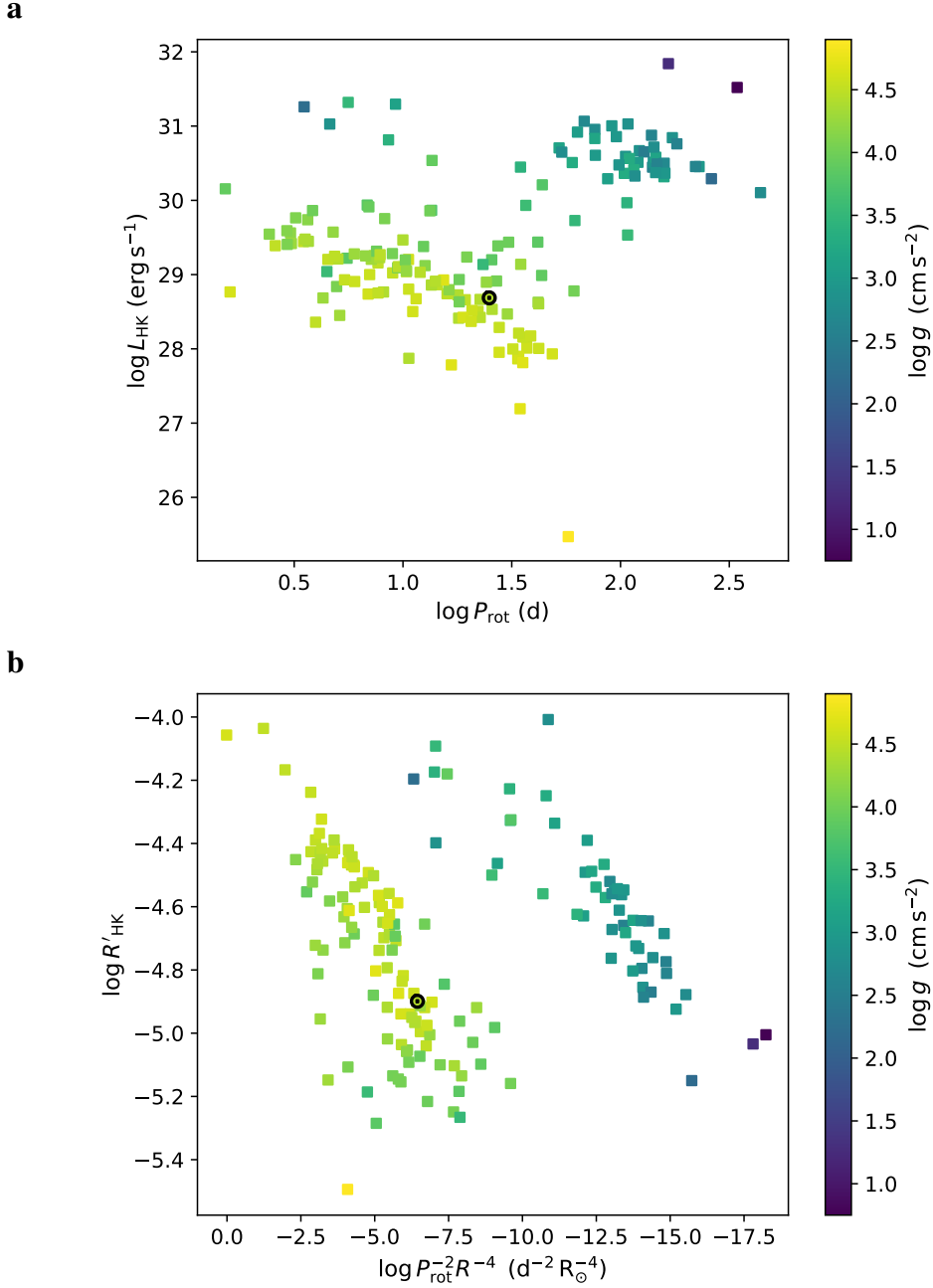


Figure 4: Suggested alternative rotation–activity relations independent of convective turnover time. a, Chromospheric Ca II H&K luminosity, $\log L_{\text{HK}}$, vs. rotation period, P_{rot} . **b,** Chromospheric activity, $\log R'_{\text{HK}}$, vs. combined rotation period and stellar radius, $P_{\text{rot}}^{-2} R^{-4}$. The colour scale for $\log g$ is the same as in Figure 2.

Methods

Chromospheric activity and astrophysical parameters. The initial sample selection consists of all the stars included in the Mount Wilson Observatory (MWO) Calcium HK Project¹⁸ that have time series observations spanning over five years and covering at least four complete observing seasons. This selection consists of 224 stars in total. Using sufficiently extended time series data like this ensures averaging over yearly activity variations and facilitates a more reliable rotation period search. The final sample for which it was possible to determine both P_{rot} and τ_c consists of 58 main sequence and 92 evolved stars. We supplemented this sample by five moderately to very active main sequence stars which have a poorer coverage in the MWO data but have accurate P_{rot} available from photometric studies²³.

The Ca II H&K emission ratios, $R'_{\text{HK}} = L_{\text{HK}}/L_{\text{bol}} = F'_{\text{HK}}/\sigma T_{\text{eff}}$, were calculated from the averaged MWO S -index observations²⁴ after removing sections of data with apparent calibration issues and outliers more than 4σ away from the sample mean²⁵. The conversion is colour dependent and defined separately for the main sequence and evolved stars²⁶. The choice of appropriate conversion law was made based on the absolute V -band magnitude M_V , so that stars with M_V more than 1 magnitude above the main sequence²⁷ were treated as evolved stars and the rest as main sequence stars. For the cooler stars with $B - V \geq 0.8$ (or $T_{\text{eff}} \leq 5300$ K) this procedure neatly separates the main sequence from the evolved stars (see Figure 1). For the hotter stars there is no clear separation between the different evolutionary stages in the Hertzsprung-Russell diagram, but this causes no issues for calculating $\log R'_{\text{HK}}$ since the two conversion laws overlap in this region²⁶.

V -band magnitudes and $B - V$ colours were adopted from the Hipparcos photometry²⁸ for all stars apart from the Sun²⁷. Parallaxes were drawn from the Gaia Data Release 2^{29–31}, where available, otherwise adopting Hipparcos parallaxes³². Interstellar extinction was assumed to be $a_V = 1.5\text{mag/kpc}$ for calculating the absolute magnitudes³³, which is a workable assumption since the stellar sample is located largely in our galactic neighborhood.

We adopted literature values for the effective temperature, T_{eff} , and luminosity, L ,^{27,34} and the metallicity, $[\text{Fe}/\text{H}]$,³⁵ of the stars. For some stars no values of T_{eff} or L were available and these had to be estimated from the photometry³⁶ and the stellar radii, R , estimated thereof³⁷. The Ca II H&K luminosities were calculated from the emission fluxes as $L_{\text{HK}} = 4\pi R^2 F'_{\text{HK}}$. Values of surface gravity, $\log g$, were compiled from the PASTEL catalogue³⁸.

Stellar structure models. Since the convective turnover time τ_c depends on the stellar mass, chemical composition, and evolutionary stage, we derived its value for each star individually using a grid of stellar evolution models from the Yale-Potsdam Stellar Isochrones¹⁹ (YaPSI). In the YaPSI models, τ_c is calculated according to a global definition³⁹ based on an average over the whole convection zone of the star.

The position of each star in the Hertzsprung-Russell diagram (i.e., $\log T_{\text{eff}}$, $\log L/L_{\odot}$) was compared with the model evolutionary tracks, and a subset of tracks matching its parameters within

the observational uncertainties was selected. We assumed uncertainties of 100 K in T_{eff} and 0.12 dex in $\log L/L_{\odot}$. A best-fitting track was then generated from the selected tracks by linear interpolation, and τ_c was extracted from this synthetic track at the point of closest approach to the observed parameters. We repeated this procedure for three different metallicities: $[\text{Fe}/\text{H}] = 0.5$, 0.0, and 0.3 (with initial helium fraction kept constant at $Y = 0.28$), obtaining an estimate of τ_c in each case. This range of $[\text{Fe}/\text{H}]$ encompasses almost the totality of the stars within our sample (Extended Data Figure 2). The final value of τ_c was obtained by linear interpolation in $[\text{Fe}/\text{H}]$. The range of τ_c obtained from the models at different metallicities was used to estimate the uncertainty on τ_c . It should be noted that although this uncertainty is only qualitative (i.e., it cannot be interpreted as a formal error bar on τ_c), we found that the stars with the largest uncertainty are those close to the $\tau_c \approx 0$ d limit, lending further support to excluding the stars with the smallest τ_c from the analysis. The uncertainties of Ro , as shown in Figure 3, were computed by propagation of uncertainty from the τ_c uncertainties and the standard deviations of the P_{rot} estimates.

For stars on the main sequence, our theoretical values of τ_c are in good qualitative agreement with the classical empirical estimates³, except for a roughly $\tau_c/\tau_{c,\text{empirical}} = 2.6$ factor between the two. For stars in the subgiant and red giant branch phases, the stellar evolution models predict a strong dependence of τ_c on the evolutionary stage of the star, which is not captured by the empirical estimates.

The evolutionary stages of the stars, indicated in Figure 3, were determined from the evolutionary track fits using the following criteria. The termination age main sequence occurs when the hydrogen mass fraction in the core of a star reaches below 10^{-4} , after which the stars enter their subgiant phase. The transition from the subgiant to the giant phase was set to occur at the bottom of the red giant branch, which was defined to be reached once the inert helium core reaches a mass of $M_{\text{He}} > 0.1M_{\odot}$.

Determining precise stellar properties for red giants by matching their observed properties to evolutionary tracks and isochrones is notoriously difficult^{40,41}. In addition, a significant source of scatter in the value of τ_c for subgiant and early red giant stars comes from their fast evolutionary timescales, and is therefore unfortunately unavoidable. This effect is illustrated in Extended Data Figure 3, which shows a selection of evolution tracks for the main sequence and post-main sequence phases and the corresponding evolution of τ_c . For stars of mass $M < 1.3M_{\odot}$, τ_c remains essentially constant during the main sequence and increases smoothly during the post-main sequence evolution. On the other hand, stars of mass $M > 1.5M_{\odot}$ have no outer convection zone in the main sequence. As they reach the bottom of the red giant branch, a sizable convective envelope develops in a much faster timescale than in their less massive counterparts. Correspondingly, τ_c changes very rapidly from zero to a few hundred days, a value typical of red giant stars.

Period analysis. The P_{rot} were determined for the stars from the rotational modulation in the MWO S -index time series, caused by the transit of chromospheric active regions over the visible stellar hemispheres²⁵. An initial period search was performed for each complete observing season using periodic Gaussian processes⁴². If the different seasons yielded repeatedly comparable period

values, these were used as initial guesses for computing the final period estimate from the full time series using the Continuous Period Search method⁴³.

Gaussian clustering. The clustering analysis of the rotation–activity diagrams was done using the Gaussian Mixture Model with Expectation Maximisation⁴⁴. We searched for the statistically most likely configuration of clusters, not assuming any prior knowledge neither about the number of clusters nor their covariances. The algorithm was run for the number of clusters ranging from one to five and the optimal configuration was determined by minimising the Bayesian Information Criterion⁴⁵. The most probable cluster membership was determined afterwards for the individual stars using Mahalanobis distance⁴⁶.

Data availability. The Mount Wilson Observatory HK Project data are available online at ftp://solis.nso.edu/MountWilson_HK/ and the Gaia Data Release 2 from the Gaia Archive at <http://gea.esac.esa.int/archive/>. The YaPSI stellar models are available at <http://www.astro.yale.edu/yapsi/>. The adopted and derived astrophysical parameters for the stellar sample used in the present study are available in online tables at the CDS astronomical data center via anonymous ftp to [cdsarc.u-strasbg.fr](ftp://cdsarc.u-strasbg.fr) (130.79.128.5) or via <http://cdsarc.u-strasbg.fr/viz-bin/qcat?J/other/NatAs>.

1. Charbonneau, P. Dynamo Models of the Solar Cycle. *Living Reviews in Solar Physics* **7**, 3 (2010).
2. Reiners, A., Basri, G. & Browning, M. Evidence for Magnetic Flux Saturation in Rapidly Rotating M Stars. *Astrophys. J.* **692**, 538–545 (2009).
3. Noyes, R. W., Hartmann, L. W., Baliunas, S. L., Duncan, D. K. & Vaughan, A. H. Rotation, convection, and magnetic activity in lower main-sequence stars. *Astrophys. J.* **279**, 763–777 (1984).
4. Gunn, A. G., Mitrou, C. K. & Doyle, J. G. On the rotation-activity correlation for active binary stars. *Mon. Not. R. Astron. Soc.* **296**, 150–164 (1998).
5. Wright, N. J., Drake, J. J., Mamajek, E. E. & Henry, G. W. The Stellar-activity-Rotation Relationship and the Evolution of Stellar Dynamos. *Astrophys. J.* **743**, 48 (2011).
6. Mamajek, E. E. & Hillenbrand, L. A. Improved Age Estimation for Solar-Type Dwarfs Using Activity-Rotation Diagnostics. *Astrophys. J.* **687**, 1264–1293 (2008).
7. Pizzolato, N., Maggio, A., Micela, G., Sciortino, S. & Ventura, P. The stellar activity-rotation relationship revisited: Dependence of saturated and non-saturated X-ray emission regimes on stellar mass for late-type dwarfs. *Astron. Astrophys.* **397**, 147–157 (2003).
8. Reiners, A., Schüssler, M. & Passegger, V. M. Generalized Investigation of the Rotation-Activity Relation: Favoring Rotation Period instead of Rossby Number. *Astrophys. J.* **794**, 144 (2014).

9. Strassmeier, K. G., Fekel, F. C., Bopp, B. W., Dempsey, R. C. & Henry, G. W. Chromospheric CA II H and K and H-alpha emission in single and binary stars of spectral types F6-M2. *Astrophys. J. Supplement Series* **72**, 191–230 (1990).
10. Vidotto, A. A. *et al.* Stellar magnetism: empirical trends with age and rotation. *Mon. Not. R. Astron. Soc.* **441**, 2361–2374 (2014).
11. Gilliland, R. L. The relation of chromospheric activity to convection, rotation, and evolution off the main sequence. *Astrophys. J.* **299**, 286–294 (1985).
12. Babcock, H. W. The Topology of the Sun's Magnetic Field and the 22-YEAR Cycle. *Astrophys. J.* **133**, 572 (1961).
13. Leighton, R. B. A Magneto-Kinematic Model of the Solar Cycle. *Astrophys. J.* **156**, 1 (1969).
14. Dikpati, M. & Charbonneau, P. A Babcock-Leighton Flux Transport Dynamo with Solar-like Differential Rotation. *Astrophys. J.* **518**, 508–520 (1999).
15. Parker, E. N. The Formation of Sunspots from the Solar Toroidal Field. *Astrophys. J.* **121**, 491 (1955).
16. Brandenburg, A. & Subramanian, K. Astrophysical magnetic fields and nonlinear dynamo theory. *Physics Reports* **417**, 1–209 (2005).
17. Skumanich, A. Time Scales for CA II Emission Decay, Rotational Braking, and Lithium Depletion. *Astrophys. J.* **171**, 565 (1972).
18. Wilson, O. C. Chromospheric variations in main-sequence stars. *Astrophys. J.* **226**, 379–396 (1978).
19. Spada, F., Demarque, P., Kim, Y.-C., Boyajian, T. S. & Brewer, J. M. The Yale-Potsdam Stellar Isochrones. *Astrophys. J.* **838**, 161 (2017).
20. Wright, N. J. & Drake, J. J. Solar-type dynamo behaviour in fully convective stars without a tachocline. *Nature* **535**, 526–528 (2016).
21. Newton, E. R. *et al.* The H α Emission of Nearby M Dwarfs and its Relation to Stellar Rotation. *Astrophys. J.* **834**, 85 (2017).
22. Wright, N. J., Newton, E. R., Williams, P. K. G., Drake, J. J. & Yadav, R. K. The stellar rotation-activity relationship in fully convective M dwarfs. *Mon. Not. R. Astron. Soc.* **479**, 2351–2360 (2018).
23. Lehtinen, J., Jetsu, L., Hackman, T., Kajatkari, P. & Henry, G. W. Activity trends in young solar-type stars. *Astron. Astrophys.* **588**, A38 (2016).
24. Egeland, R. *et al.* The Mount Wilson Observatory S-index of the Sun. *Astrophys. J.* **835**, 25 (2017).

25. Olsper, N., Lehtinen, J. J., Käpylä, M. J., Pelt, J. & Grigorievskiy, A. Estimating activity cycles with probabilistic methods. II. The Mount Wilson Ca H&K data. *Astron. Astrophys.* **619**, A6 (2018).
26. Rutten, R. G. M. Magnetic structure in cool stars. VII - Absolute surface flux in CA II H and K line cores. *Astron. Astrophys.* **130**, 353–360 (1984).
27. Cox, A. N. (ed.) *Allen’s astrophysical quantities* (Springer, 2000). 4th edn.
28. ESA (ed.). *The HIPPARCOS and TYCHO catalogues. Astrometric and photometric star catalogues derived from the ESA HIPPARCOS Space Astrometry Mission*, vol. 1200 of *ESA Special Publication* (1997).
29. Gaia Collaboration *et al.* The Gaia mission. *Astron. Astrophys.* **595**, A1 (2016).
30. Gaia Collaboration *et al.* Gaia Data Release 2. Summary of the contents and survey properties. *Astron. Astrophys.* **616**, A1 (2018).
31. Luri, X. *et al.* Gaia Data Release 2. Using Gaia parallaxes. *Astron. Astrophys.* **616**, A9 (2018).
32. van Leeuwen, F. Validation of the new Hipparcos reduction. *Astron. Astrophys.* **474**, 653–664 (2007).
33. Vergely, J. L., Egret, D., Freire Ferrero, R., Valette, B. & Koeppen, J. The Extinction in the Solar Neighbourhood from the HIPPARCOS Data. In Perryman, M. A. C. *et al.* (eds.) *Hipparcos - Venice ’97*, vol. 402 of *ESA Special Publication*, 603–606 (1997).
34. Andrae, R. *et al.* Gaia Data Release 2. First stellar parameters from Apsis. *Astron. Astrophys.* **616**, A8 (2018).
35. Gáspár, A., Rieke, G. H. & Ballering, N. The Correlation between Metallicity and Debris Disk Mass. *Astrophys. J.* **826**, 171 (2016).
36. Flower, P. J. Transformations from Theoretical Hertzsprung-Russell Diagrams to Color-Magnitude Diagrams: Effective Temperatures, B-V Colors, and Bolometric Corrections. *Astrophys. J.* **469**, 355 (1996).
37. Gray, D. F. *The observation and analysis of stellar photospheres* (Cambridge University Press, 2005).
38. Soubiran, C., Le Campion, J.-F., Brouillet, N. & Chemin, L. The PASTEL catalogue: 2016 version. *Astron. Astrophys.* **591**, A118 (2016).
39. Kim, Y.-C. & Demarque, P. The Theoretical Calculation of the Rossby Number and the “Nonlocal” Convective Overturn Time for Pre-Main-Sequence and Early Post-Main-Sequence Stars. *Astrophys. J.* **457**, 340 (1996).

40. Serenelli, A. M., Bergemann, M., Ruchti, G. & Casagrande, L. Bayesian analysis of ages, masses and distances to cool stars with non-LTE spectroscopic parameters. *Mon. Not. R. Astron. Soc.* **429**, 3645–3657 (2013).
41. Silva Aguirre, V. & Serenelli, A. M. Asteroseismic age determination for dwarfs and giants. *Astronomische Nachrichten* **337**, 823 (2016).
42. Wang, Y., Khardon, R. & Protopapas, P. Nonparametric Bayesian Estimation of Periodic Light Curves. *Astrophys. J.* **756**, 67 (2012).
43. Lehtinen, J., Jetsu, L., Hackman, T., Kajatkari, P. & Henry, G. W. The continuous period search method and its application to the young solar analogue HD 116956. *Astron. Astrophys.* **527**, A136 (2011).
44. Barber, D. *Bayesian Reasoning and Machine Learning* (Cambridge University Press, 2012).
45. Stoica, P. & Selen, Y. Model-order selection: a review of information criterion rules. *IEEE Signal Processing Magazine* **21**, 36–47 (2004).
46. Mahalanobis, P. C. On the generalized distance in statistics. *Proc. Nat. Inst. of Sciences of India* **2**, 49 (1936).

Acknowledgements This work has made use of data from the European Space Agency (ESA) mission *Gaia* (<https://www.cosmos.esa.int/gaia>), processed by the *Gaia* Data Processing and Analysis Consortium (DPAC, <https://www.cosmos.esa.int/web/gaia/dpac/consortium>). Funding for the DPAC has been provided by national institutions, in particular the institutions participating in the *Gaia* Multilateral Agreement.

The chromospheric activity data derive from the Mount Wilson Observatory HK Project, which was supported by both public and private funds through the Carnegie Observatories, the Mount Wilson Institute, and the Harvard-Smithsonian Center for Astrophysics starting in 1966 and continuing for over 36 years. These data are the result of the dedicated work of O. Wilson, A. Vaughan, G. Preston, D. Duncan, S. Baliunas, and many others.

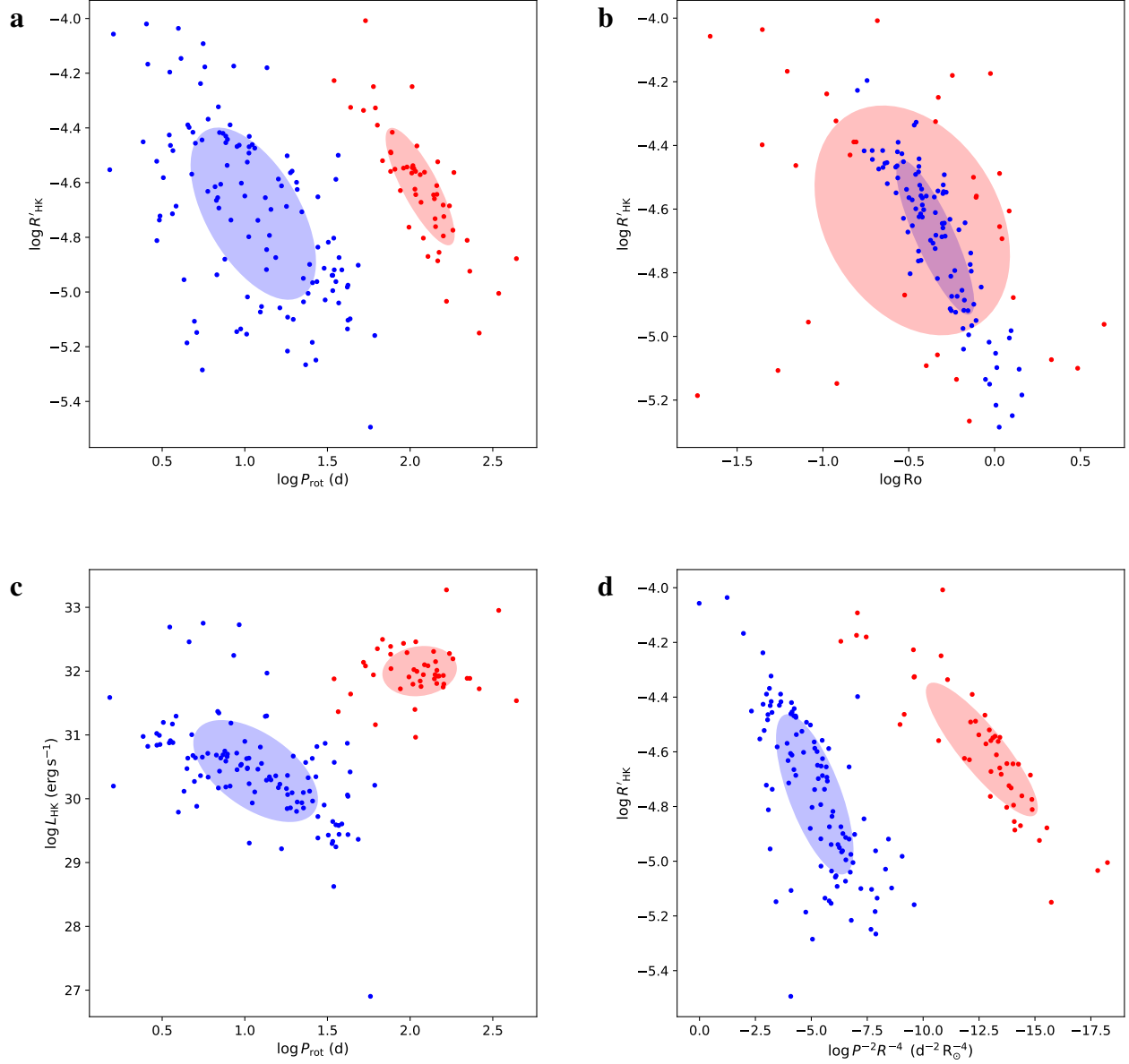
The work has made use of the SIMBAD database at CDS, Strasbourg, France, and NASA’s Astrophysics Data System (ADS) services.

J.J.L. acknowledges financial support from the Independent Max Planck Research Group “SOLSTAR”. F.S. acknowledges the support of the German space agency (Deutsches Zentrum für Luft- und Raumfahrt) under PLATO Data Center grant 500O1501. M.J.K., N.O., and P.J.K. acknowledge the support of the Academy of Finland ReSoLVE Centre of Excellence (grant number 307411). P.J.K. acknowledges support from DFG Heisenberg grant (No. KA 4825/2-1). This project has received funding from the European Research Council (ERC) under the European Union’s Horizon 2020 research and innovation programme (Project UniSDyn, grant agreement n:o 818665).

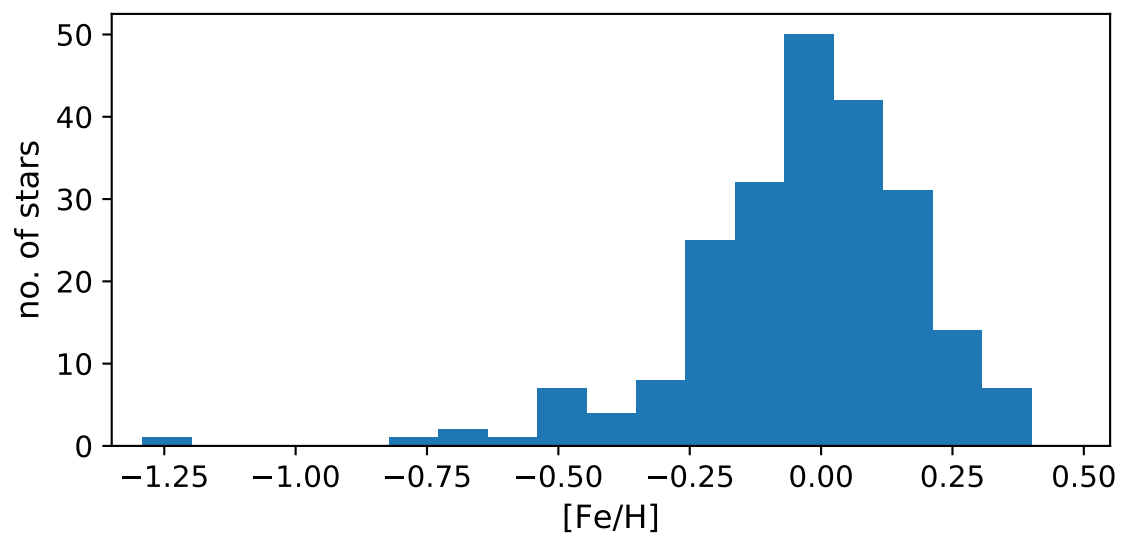
Author contributions All authors contributed to the research and its design. J.J.L. and N.O. led the data analysis of the observations. F.S. led the stellar structure modelling. M.J.K. and P.J.K. led the theoretical interpretation of the obtained results. All authors contributed to the discussion of the results and to the manuscript.

Competing interests The authors declare no competing interests.

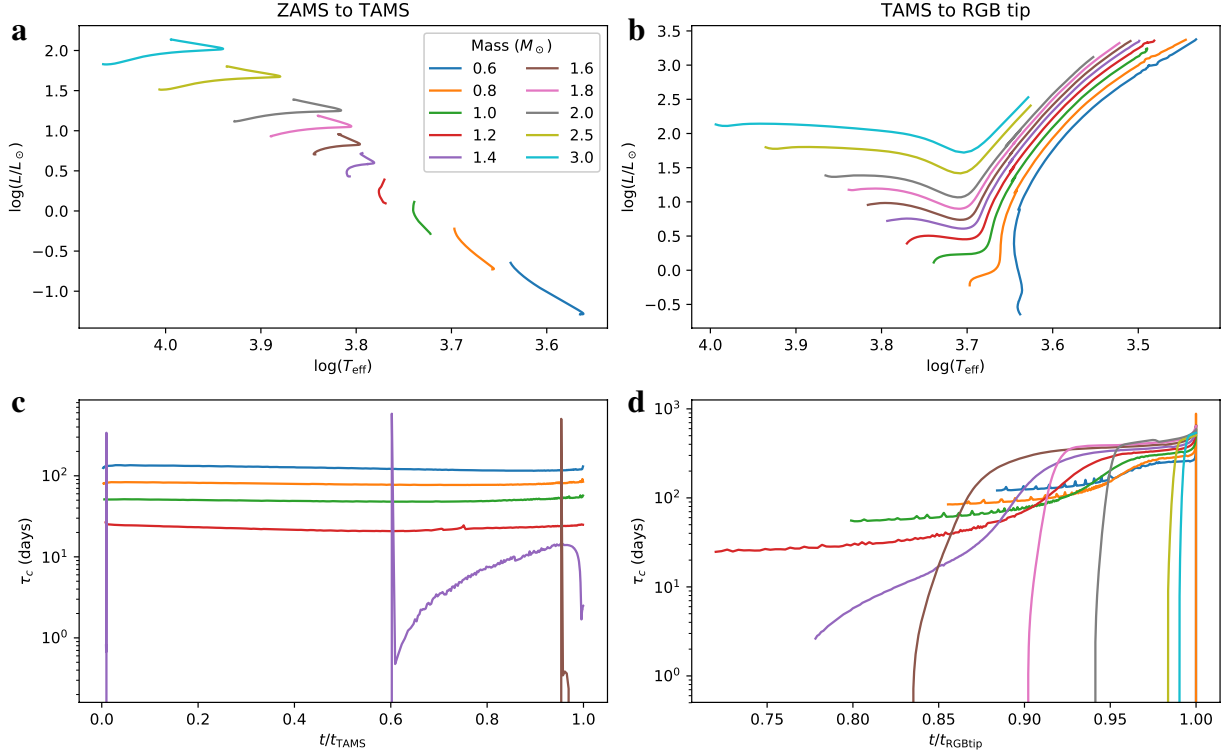
Author information Reprints and permissions information is available at www.nature.com/reprints. Correspondence and requests for materials should be addressed to J.J.L. (lehtinen@mps.mpg.de).



Extended Data Figure 1: Gaussian clustering for the rotation–activity relation. **a**, Chromospheric activity, $\log R'_{\text{HK}}$, vs. rotation period, $\log P_{\text{rot}}$. **b**, Chromospheric activity, $\log R'_{\text{HK}}$, vs. Rossby number, $\log \text{Ro}$. **c**, Chromospheric Ca II H&K luminosity $\log L_{\text{HK}}$ vs. rotation period, $\log P_{\text{rot}}$. **d**, Chromospheric activity, $\log R'_{\text{HK}}$, vs. combined rotation period and stellar radius, $\log P_{\text{rot}}^{-2} R^{-4}$. Optimal clustering of the data is indicated by the blue and red ellipses, reflecting the corresponding 95% confidence regions. The individual stars are coloured according to their inferred cluster membership.



Extended Data Figure 2: Metallicity distribution of the sample stars.



Extended Data Figure 3: Selected stellar evolution tracks with the time evolution of convective turnover time, τ_c . **a**, Evolution in the Hertzsprung-Russell (HR) diagram from the zero age main sequence (ZAMS) to the termination age main sequence (TAMS). **b**, Evolution in the HR diagram from TAMS to the red giant branch (RGB) tip. **c**, Evolution of τ_c from ZAMS to TAMS. **d**, Evolution of τ_c from TAMS to RGB tip. All ages are normalised to TAMS or RGB tip age.